

9-14-2013

Near sputter-threshold GaSb nanopatterning

Osman El-Atwani

Birck Nanotechnology Center, Purdue University, oelatwan@purdue.edu

Sean Gonderman

Birck Nanotechnology Center, Purdue University, sean14@purdue.edu

Jean Paul Allain

Birck Nanotechnology Center, Purdue University, allain@purdue.edu

Follow this and additional works at: <http://docs.lib.purdue.edu/nanopub>

 Part of the [Nanoscience and Nanotechnology Commons](#)

El-Atwani, Osman; Gonderman, Sean; and Allain, Jean Paul, "Near sputter-threshold GaSb nanopatterning" (2013). *Birck and NCN Publications*. Paper 1465.

<http://dx.doi.org/10.1063/1.4820261>

This document has been made available through Purdue e-Pubs, a service of the Purdue University Libraries. Please contact epubs@purdue.edu for additional information.

Near sputter-threshold GaSb nanopatterning

Osman El-Atwani, Sean Gonderman, and Jean Paul Allain

Citation: [Journal of Applied Physics](#) **114**, 104308 (2013); doi: 10.1063/1.4820261

View online: <http://dx.doi.org/10.1063/1.4820261>

View Table of Contents: <http://scitation.aip.org/content/aip/journal/jap/114/10?ver=pdfcov>

Published by the [AIP Publishing](#)



Re-register for Table of Content Alerts

Create a profile.



Sign up today!



Near sputter-threshold GaSb nanopatterning

Osman El-Atwani,^{1,2,3,a)} Sean Gonderman,² and Jean Paul Allain^{1,2,3}

¹*School of Materials Engineering, Purdue University, West Lafayette, Indiana 47907, USA*

²*School of Nuclear Engineering, Purdue University, West Lafayette, Indiana 47907, USA*

³*Birck Nanotechnology Center, Purdue University, West Lafayette, Indiana 47907, USA*

(Received 22 July 2013; accepted 18 August 2013; published online 12 September 2013)

Nanopatterning at sputter-threshold energies with Ar irradiation of GaSb (100) surfaces is presented. Comparison with high-energy irradiations up to 1000 eV is conducted measuring *in-situ* the composition evolution over irradiation time at early stages (e.g., $<10^{17}$ cm⁻²) and up to nanostructure saturation (e.g., $\sim 10^{18}$ cm⁻²). Low-energy irradiation is conducted for energies between 15–100 eV and a low-aspect ratio nanostructured dot formation is found. Furthermore, the role of oxide on GaSb is found to delay nanostructure formation and this is predominant at energies below 100 eV. *In-situ* quartz crystal microbalance measurements collect sputtered particles yielding the sputter rate at threshold energies indicating a correlation between erosion and surface composition consistent with recent theoretical models. Ion-induced segregation is also found and indicated by both compositional measurements of both the surface and the sputtered plume. © 2013 AIP Publishing LLC. [<http://dx.doi.org/10.1063/1.4820261>]

I. INTRODUCTION

The use of ion beam sputtering (IBS) has resulted in the formation of nanostructures of different shapes and sizes on semiconductor surfaces.^{1–6} More recently, nanopatterning by ion-beam irradiation on GaSb by Facsko *et al.*⁷ demonstrated that 420 eV argon irradiation resulted in hexagonally ordered nanodots (short pillars). These results along with many others⁸ pointed to the potential of IBS as an alternative maskless nanofabrication parallel technique. However, understanding the formation mechanism and discovering the correlation between the characteristic parameters (shape, characteristic, length, and size) and the irradiation conditions are critical to elucidate the steps to reliably achieve nanopattern formation. IBS has been shown to lead to size-dependent nanostructures by variation of the incident particle energy.⁹ In particular, as the energy decreased, the average nanostructure size and correlated spacing between nanostructures decreased. Therefore, as device feature size approaches the sub-20 nm scale, working at low IBS energies becomes indispensable. Moreover, understanding the fundamental mechanisms of low-energy IBS and nanopattern formation on III–V semiconductors demands the use of *in-situ* characterization techniques that are able to couple surface composition with nanopatterning control. This work presents for the first time *in-situ* measurements of IBS nanopatterned GaSb(100) that correlates surface composition, structure, and incident particle energy near the sputter threshold to nanopatterning.

The nanostructures observed by Facsko *et al.*⁷ were conjectured to consist of nanodots. The formation of these nanodots via ion beam irradiation at normal incidence was described as a balance between the surface instability

induced by the ion beam via sputtering and the smoothing effect due to surface diffusion. This model is described with the Kuramoto-Sivashinsky (KS) equation.¹⁰ It was reported,⁷ however, that in the temperature range between -60 °C and $+60$ °C, diffusion is dominated by the effective ion-induced surface diffusion.

Several studies were performed to explain the physical mechanism of nanostructure formation on GaSb via ion beam irradiation at normal incidence. Facsko *et al.*¹¹ suggested the formation mechanism was preferential sputtering of antimony (Sb) that led to the surface instability during irradiation. A mechanism of preferential sputtering of Sb raised some doubts however. In addition to the fact that there was no direct experimental evidence of Sb being preferentially sputtered, SRIM¹² calculations based on a linear cascade and a binary collision approximation (BCA) have shown both Ga and Sb sputters at the same magnitude.¹³

Le Roy *et al.*^{14,15} suggested another mechanism that is based on Ga surface segregation to the surface during the early stage growth stages of the structures. According to this study, Ga segregates to the surface and form Ga shields (islands) on the surface. Segregation of Ga is claimed to occur due to the preferential sputtering of Sb. As the structures begin to develop, segregation of Ga to the tip of the nanostructures provide the supply of Ga to support the shielding effect. While the results of the paper demonstrated the formation of pillars instead of dots, the suggested mechanism was based on an *ex-situ* x-ray photoelectron spectroscopy (XPS) study. Recently, El-Atwani *et al.*¹³ demonstrated that *ex-situ* results lead to higher Ga surface compositions during early stage structure formation due to the role of native oxides on the surface. Moreover, the study showed that if the samples were exposed to atmosphere prior to characterization, oxides created from the ambient air could drive Ga to the surface inadvertently. By comparing *in-situ* and *ex-situ* XPS and low energy ion scattering spectroscopy

^{a)}Author to whom correspondence should be addressed. Email: oelatwan@purdue.edu. Telephone: +1 765 409 8186. Present address: Nuclear Engineering, Purdue University, 400 Central drive, West Lafayette, Indiana 47907, USA.

(LEISS) studies, El-Atwani *et al.*¹⁶ demonstrated that higher relative Ga composition on the surfaces observed during *ex-situ* XPS studies was correlated to high Ga₂O₃ relative fractions. In recent work, Bradley and Shipman^{17,18} introduced a model (noted as the BS Model) that elucidated the mechanism leading to hexagonal ordered nanostructures by IBS. According to the model, the ion beam induced a change in the composition due to preferential sputtering of one element. The preferentially sputtered element is situated on the peaks of the nanostructures. The coupling between the altered composition layer and the morphology can induce this surface instability. It was demonstrated that in this case, Sb is preferentially sputtered and thus, Sb is situated on the peaks of the nanostructures during early stage formation at fluences less than approximately 10^{17} cm⁻² for Ar⁺ irradiation. However, in the BS model, the coupling between surface composition and nanoscale topography requires that the binary system contain dissimilar sputter yields for each component and a non-negligible momentum induced from incident ions to surface atoms. Scott Norris¹⁹ reported a new model, introducing an alternate mechanism that could help explain patterning of binary component systems (i.e., GaSb). A chemically driven surface instability was found to induce GaSb nanopatterning by phase separation of Ga and Sb atoms. This approach allows the possibility that the same component is *both* preferentially sputtered *and* redistributed; in this case Sb. More importantly, this model accounts for a non-Fickian approach to the surface transport of adatoms, which likely resembles more closely the real condition of GaSb under room-temperature irradiation. Thus, according to Norris' model, Ga enriches the peaks of the nanostructures and Sb is found predominantly in the valleys (or troughs between the pillar nanostructures). That is, the composition variations are out of phase with the height variations.

The primary conclusion from the discussion above on computational modeling of GaSb nanopatterning is that the surface composition is directly coupled with the morphological changes that occur on the samples during irradiation. Furthermore, the surface composition during early stage nanostructure growth and past the structure amplitude saturation (defined as the invariance of nanostructure size with fluence) can yield critical information to guide understanding of nanostructure formation.

In this paper, a collection of *in-situ* experiments that combine measurements of the relative surface composition of Ga and surface structure was performed for the first time on GaSb substrates during irradiation at low (near sputtering threshold <80 eV) and high energies (up to 1000 eV). The relative surface composition of Ga was calculated from both low-energy ion scattering spectroscopy (LEISS) and x-ray photoelectron spectroscopy (XPS) at different fluences during the irradiation. This work also examines the possibility of nanopatterning at GaSb sputter threshold energies. Another unique aspect of this work is measurement *in-situ* of the erosion rate and composition of sputtered plume using a particle-collection scheme. Furthermore, correlation of nanostructure formation with irradiation fluence is achieved with real-time growth behavior of GaSb nanostructures during

low-energy argon irradiation with *in-situ* real-time grazing incidence small angle x-ray scattering (GISAXS).

II. EXPERIMENTAL SETUP

Irradiation and characterization of the samples were performed in the Particle and Radiation Interaction of Hard and Soft Matter (PRIHSM) facility at Purdue University. A gridded, non-reactive ion source (Tetra Gen II) was used to irradiate the samples. Irradiations were performed at several energies ranging from 25–1000 eV. All the irradiations were performed at normal incidence. The irradiation flux varied between $0.7\text{--}3 \times 10^{14}$ cm⁻² s⁻¹ depending on the particle's incident energy.

XPS was performed at normal emission of photoelectrons with a source-analyzer angle of 54.7°. The excitation source was Mg K α (1253.4 eV). The anode voltage and the emission current were 13 keV and 15.0 mA, respectively. LEISS was performed using He ions at 1500 eV (flux of $1\text{--}3 \times 10^{13}$ cm⁻² s⁻¹) and a backscattering angle of 145°. The operating pressure was under 2×10^{-8} torr and the partial pressure of oxygen was under 9×10^{-11} torr as read from the residual gas analyzer (RGA). For the high-energy experiments, the samples were kept at room temperature using a combination of liquid nitrogen cooling and a resistive heater. XPS and LEISS characterization were conducted under *in-situ* conditions using a VG Scienta R3000 energy and momentum dispersive particle analyzer. LEISS probes primarily the first monolayer or the so-called sputter depth where most sputtered atoms are derived. This region is also known to be amorphous during the irradiation process. XPS probes around 8-nm from the vacuum/material interface and thus provides information of impurity diffusion from the subsurface (e.g., >1-nm) to the first layer of atoms at the surface.

For irradiations less than 100 eV, the oxide layer hinders the structure formation process.¹⁶ It was reported^{20,21} that etching GaSb substrates with 1:1 hydrochloric acid-methanol solution reduces the thickness of the native oxide layer to about 1.7-nm. As mentioned in our previous work,¹⁶ to prepare a completely oxide-free GaSb sample, the etching procedure above was necessary.

In-situ erosion rate measurements (at different energies) were performed using a single crystal Quartz Crystal Microbalance (QCM). Use of QCM as an *in-situ* erosion rate measurement during irradiation of GaSb enabled correlations with erosion rate, surface composition, structure, and size. A decrease in the frequency of the quartz crystal resonator (microbalance) signifies the collection of mass sputtered from the irradiated GaSb sample. In addition to the erosion rate, the composition of the sputtered plume was desired.

The sputtering collection experiment was performed as follows. A silicon wafer coated with an atomically smooth (~ 0.4 nm RMS roughness) rhodium thin film sample (1 cm²) was inserted into the chamber and irradiated to clean the oxide layer. The Rh/Si sample was then located facing the GaSb sample at an optimal collection angle and left to collect the sputtered atoms while the GaSb is irradiated. The optical collection angle was selected to maximize sputtered

atom collection and minimize occlusion of the irradiation beam. Collection of the sputtered atoms was performed at 1–2 min time intervals. Post-irradiation, *in-situ* XPS measurement was performed on the Rh/Si sample to determine the composition of the collected particles. The effect of reflected Ga or Sb sputtered particles arriving at the Rh/Si surface was assessed by running low-energy incident particle reflection simulations using SRIM 2008. At the most probable sputtered energies of 2–3 eV, the backscattered Ga, Sb particles were equal to zero. For higher energy species, the backscattered reflection varied between 0.1%–5% for energies between 10–100 eV (much higher than expected for the sputtered energy distribution of Ga and Sb atoms). Therefore, this effect is negligible and the sputtered plume distribution can in fact be collected and measured *in-situ* with our collection methodology.

Real time grazing incidence small angle x-ray scattering (GISAXS) was performed on beam line X21 of the National Synchrotron Light Source (NSLS) at Brookhaven National laboratory (BNL). The GISAXS incident x-ray angle was 0.8° and the exit angle was 0.2° . The x-ray energy was 10 keV. The irradiation for the GISAXS and XRF studies was performed in a high vacuum chamber using the same ion source (Tetra GenII) as in the other experiments. The pressure during irradiation was $8\text{--}9 \times 10^{-4}$ torr, and the irradiation was performed at normal incidence with 50 eV argon ions. The ion beam fluxes were in the range of $1\text{--}2 \times 10^{14} \text{ cm}^{-2} \text{ s}^{-1}$.

Quantification of LEISS and XPS spectra^{22–24} were performed using IGOR and CASA-XPS software packages, respectively. The relative composition was then determined as follows:

$$y = \frac{A_{\text{Ga}}/\sigma_{\text{Ga}}}{A_{\text{Ga}}/\sigma_{\text{Ga}} + A_{\text{Sb}}/\sigma_{\text{Sb}}},$$

where A_{Ga} and A_{Sb} are the areas under the curves of Ga and Sb, respectively, and σ_{Ga} and σ_{Sb} are the laboratory cross-sections of Ga and Sb, respectively.

To minimize the errors from inelastic mean free path differences and the transmission function of the analyzer, the quantification included Ga3d and Sb4d peaks, which have binding energies very close to each other (less than 15 eV). For quantification of the XPS spectra and conversion to composition, the average Scofield's relative sensitivity factors were used (1.19 for Ga3d and 2.98 for Sb4d). The Ga3d peak was always accompanied by an intrinsic loss peak at binding energy values of 6 eV or higher. Unlike extrinsic losses, intrinsic losses should be included in the quantification of the XPS spectra when extracting/reducing compositions.

III. RESULTS AND DISCUSSION

A. Surface composition vs irradiation fluence

Determining the surface compositions during the irradiation process as a function of fluence (before and during the structure growth) can help decipher the underlying mechanisms for patterning as well as validate competing theoretical and computational models. Moreover, the change in surface composition during the irradiation process, as a function of

energy, can give insight whether the formation mechanism is energy dependent specifically at energies near the sputtering threshold of GaSb under Ar irradiation.

Figure 1 shows Ga relative composition as a function of fluence at different irradiation energies ranging from low (25 eV) to high (1000 eV) energies. The irradiations were performed at normal incidence. The surface compositions were determined under *in-situ* conditions (the sample were not exposed to atmosphere before the characterization), and using XPS and LEISS. The importance of *in-situ* conditions to help elucidate correlations between surface chemistry, composition, and nanopatterning was previously reported by our group.¹⁶ While LEISS gives information regarding the surface composition in the first monolayer,^{25,26} XPS probing depth depends on the binding energies of the quantified peaks. Since Sb 4d and Ga 3d peaks were used in the quantification process, the probing depth is calculated to be 8-nm. In this case, XPS quantification provides information about the composition of the amorphous layer (ion energy induced) and the crystalline layer beneath. Using SRIM, the thickness of the amorphous layer ranges from 1-nm (at 25 eV) to 6-nm (at 1000 eV).

From the LEISS data in Figure 1, the Ga relative compositions vary at very low fluences ($1 \times 10^{15} \text{ cm}^{-2}$). This is due to the difference in the surface compositions for the samples prior to irradiation. *Ex-situ* SEM results (for another set of samples), not shown here, demonstrated that no structure formation is measured at this stage. At $5 \times 10^{15} \text{ cm}^{-2}$, the Ga relative composition is nearly the same for all energies (around 57%) and it stays nearly the same at 1 and $5 \times 10^{16} \text{ cm}^{-2}$. At fluences higher than $1 \times 10^{17} \text{ cm}^{-2}$, the Ga relative composition begins to drop slowly approaching a 1:1 Ga:Sb composition. *Ex-situ* SEM and real time GISAXS experiments²⁷ determined the early stage fluence for onset of nanostructure formation to range from $1 \times 10^{16} \text{ cm}^{-2}$ (500 eV) to $3 \times 10^{16} \text{ cm}^{-2}$ (e.g., for energies less than 100 eV). Since LEISS probes the first monolayer from which the sputtered atoms emanate, the enrichment of Ga at the GaSb sample surface during the early stage growth could be

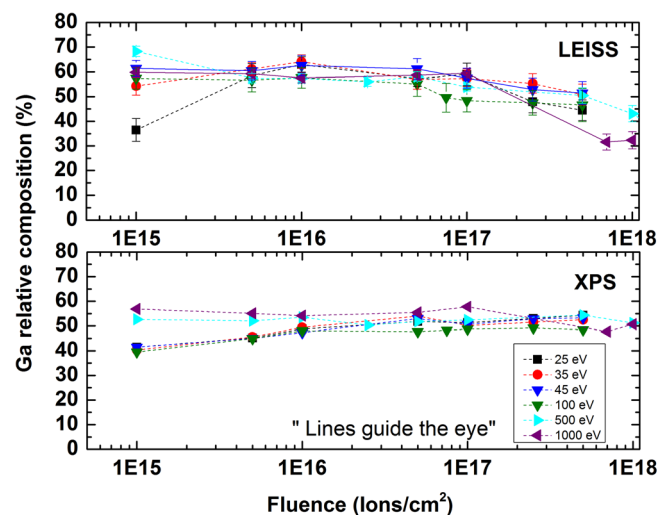


FIG. 1. *In-situ* measurements of Ga relative composition as a function of fluence determined from XPS and LEISS spectra at different irradiation energies (25, 35, 45, 100, 500, and 1000 eV). Irradiation was performed at normal incidence using argon ion beam.

a sign of preferential sputtering of Sb. The increase in the Ga relative composition during the early fluence stages is also observed in the XPS data. Higher enrichments were observed at high irradiation energies (500 and 1000 eV), where the amorphous layer thickness is larger. According to SRIM (which is based on binary collision approximation model, BCA), Ga and Sb erode at the same rate with moderate energies and Ga preferentially sputters at energies near the sputtering threshold (50–25 eV). Our results at very low energies resulted in no Sb enrichment on the surface and thus inconsistent with SRIM results.

B. Correlation between sputtered-atoms composition and surface composition

In collection experiments, we performed (described in details in Sec. II) the sputtered atoms are collected at different fluences on the rhodium-coated Si samples followed by surface characterization with XPS. These results determined that Sb is sputtered more at both 100 and 500 eV (Figure 2). In our experiments, nanostructure formation begins at a fluence of over $1 \times 10^{16} \text{ cm}^{-2}$ after which the structures begin to evolve, suggesting preferential sputtering of Sb to play a role in the formation mechanism. Sb, however, continues to sputter more (observed in our collector results from Fig. 2) after nanostructure formation even at fluences where LEISS and XPS showed a Ga to Sb ratio of 50:50 (fluences of $1.0\text{--}2.5 \times 10^{17} \text{ cm}^{-2}$). At steady state, under conditions where preferential sputtering is present, the sputtered atoms of the elements should be equal. This discrepancy may be explained by the presence of more Sb located at the valleys (or troughs) in between the nanopillars. According to the Bradley Harper model,²⁸ atoms in the valleys sputter more than atoms on the tips. Despite preferential sputtering of Sb, the higher Ga composition on the first 8-nm (XPS results) during early stages of nanostructure growth is clearly observed at fluences below 10^{17} cm^{-2} . At high energies (500 and 1000 eV), *in-situ* surface composition measurements suggest that ion-induced Sb segregation replenishes the

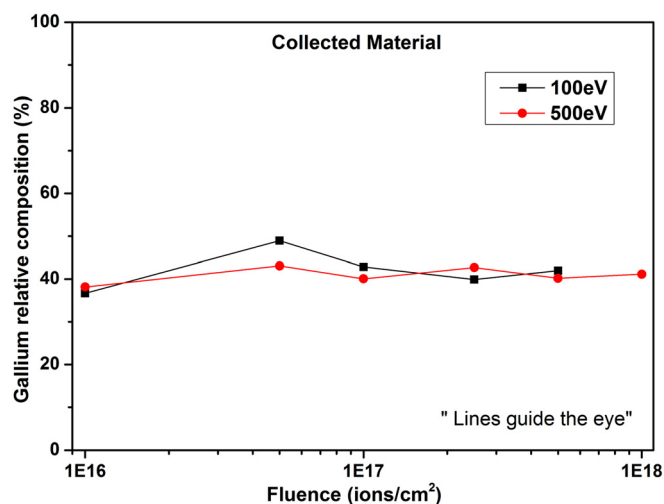


FIG. 2. Ga relative composition of the collected sputtered atoms on a rhodium-coated silicon collection sample during the irradiation of GaSb at 100 and 500 eV argon ion incident particle energies. The relative composition was determined from the *in-situ* XPS spectra of collected material.

surface. As mentioned above, the change in surface composition and the preferential sputtering of Sb before nanostructure formation (determined by *ex-situ* SEM and real time GISAXS experiments) suggest that surface chemical instability leads to nanostructure formation (morphological instability) as alluded by Norris¹⁹ to be a chemically driven surface instability mechanism induced by phase separation. This model allows for the same element to be preferentially sputtered and redistributed (in this case Sb). Contrary to the B-S model, the chemical surface instability mechanism in Norris' model does not require very different sputter yields of the elements in the binary compound. Moreover, the preferential sputtering of Sb can be enabled by Sb segregation to the surface.^{22,29} The segregation of Sb is likely non-Fickian although composition-driven diffusion may also be active. Both can be enhanced by ion irradiation but one should caution that these operate at very different time scales. An enhanced Gibbsian segregation-like³⁰ segregation is not unexpected. Gibbsian segregation is driven by a difference in surface free energies of the components at the surface. The species of lower surface energy tends to segregate to the free surface compared to the species with lower surface energy.²⁹ Sb has lower surface free energy than Ga (0.403 J/m² and 0.784 J/m² for Sb and Ga, respectively, at the melting point), hence, segregation of Sb to the surface is thermodynamically favored. If phase separation occurs, Gibbsian segregation is also expected to happen. The temperature needed to drive phase separation and/or Gibbsian segregation could be correlated to the energy transferred and deposited by the incident energetic particles. This dependence on energy and mass will be examined in future work.

Additionally, at high energies (500 and 1000 eV) and very high fluences (greater than $5 \times 10^{17} \text{ cm}^{-2}$), Sb enrichment in the ISS data is evident. A drop in the Ga relative composition is also observed from the XPS data. It should be noted at these fluences, the height of the nanostructures formed (pillars)³¹ is very large (larger than 150 nm) and this affects probing regions of the ions in the LEISS experiment. Figure 3 shows the SEM micrographs of samples irradiated at 100, 500, 1000, and also 1500 eV). The fluence was

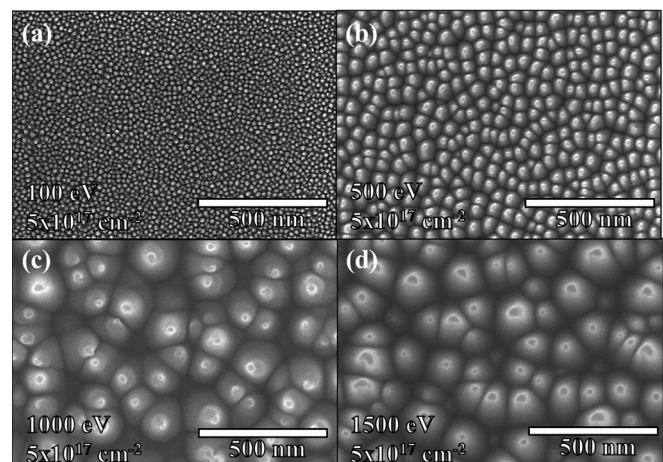


FIG. 3. Scanning electron microscopy micrographs of GaSb samples irradiated at (a)100 eV, (b) 500 eV, (c)1000 eV, and (d)1500 eV using argon ion beam to a fluence of $5 \times 10^{17} \text{ cm}^{-2}$.

$5 \times 10^{17} \text{ cm}^{-2}$. The difference in the size of the structures as the energy goes higher than 100 eV can be observed. The drop in the Ga relative composition at very high fluences is associated with the fact that ISS is not probing the valleys (due to the high aspect ratio of the pillars) but part of the sides and the top of the pillars. Angular resolution LEISS data showed different Ga relative composition between the top and the sides of the pillars. It can be concluded, however, that the pillars have different surface composition and that surface composition can affect nanostructure formation. Future work will be performed to calibrate the experiment and decipher which regions of the pillars are probed as the angle between the normal of the sample and the normal of the gun is changed during the angular resolution experiment.

C. Nanopatterning with energies near sputtering threshold

The increase in the nanostructure size and coarsening of the nanostructures as demonstrated in Fig. 3 motivated the use of low-energy ions. However, as the energy approaches the sputtering threshold, removing the sample oxide (which hinders the structure formation)¹⁶ is necessary. Our group recently reported a method resulting in a completely oxygen-free GaSb surface.¹⁶ Only by removing the native oxide layer, structuring will be possible at very low energies (25 eV). Figure 4 shows the SEM images of two sets of samples irradiated at 25, 35, and 45 eV. One set had a native oxide layer (set of images on third column: c, f, and i) and the other was completely free from oxygen prior to irradiation

(remaining images). Irradiations were performed up to a fluence of $5 \times 10^{17} \text{ cm}^{-2}$. Structuring of 25 eV was only possible on the oxygen-cleaned sample before irradiation. Cross section imaging of the oxygen-cleaned and irradiated samples shows nanostructure formation with low-aspect ratio shapes (nanoscale dots) instead of high-aspect ratio pillars as previously reported at higher energies.¹⁴ From Figure 1, it is noticeable that the Ga relative composition as a function of fluence shows similar behavior at low and high energies suggesting no difference in the formation mechanism. While it is known that sputtering on GaSb substrates occurs at high energies, SRIM predicts no sputtering at 25 eV. In order to check whether at these low energies sputtering of GaSb occurred or not, *in-situ* QCM monitoring was performed on the samples measuring *in-situ* the erosion rate during exposures.

Figure 5 shows the change in the slope of the QCM as the irradiation energy is changed from 15 to 45 eV. A collection experiment performed at 15 eV irradiation showed Ga and Sb present on the Rh/Si collector samples. The results demonstrate that even 15 eV argon ions can sputter GaSb surfaces, and thus sputtering occurred during the nanostructure formation of GaSb at energies equal to 25 eV and below.

D. Nanostructures growth behavior at energies near sputtering threshold

In order to study the structure growth behavior during the irradiation process, a real time GISAXS study was

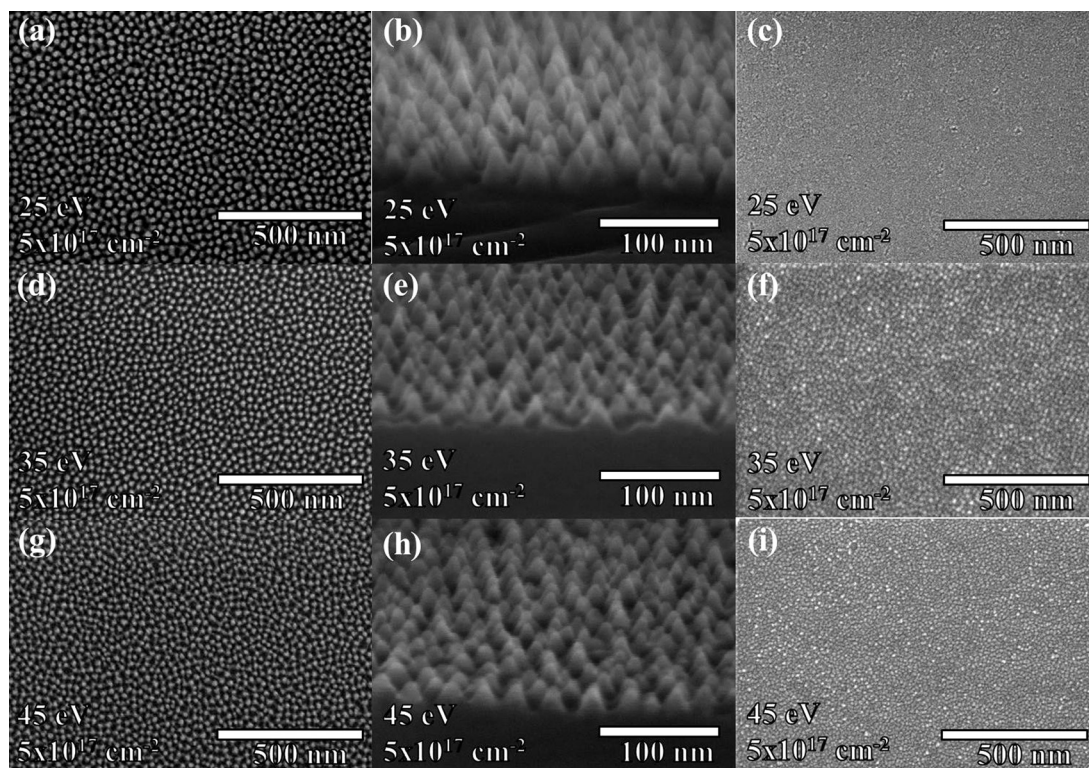


FIG. 4. Scanning electron microscopy micrographs of low energy irradiated GaSb substrates. First column: (a), (d), and (g) the samples were native oxide-free samples (oxygen cleaned) prior to irradiation and were irradiated at 25 eV, 35 eV, and 45 eV, respectively, using argon ions beam. Second column: (b), (e), and (h) cross sections images of (a), (d), and (g), respectively. Third column: (c), (f), and (i) the samples had a native oxide prior irradiation (not oxygen cleaned) and were irradiated at 25 eV, 35 eV, and 45 eV, respectively, using argon ion beam. The fluence was the $5 \times 10^{17} \text{ cm}^{-2}$ for all the samples.

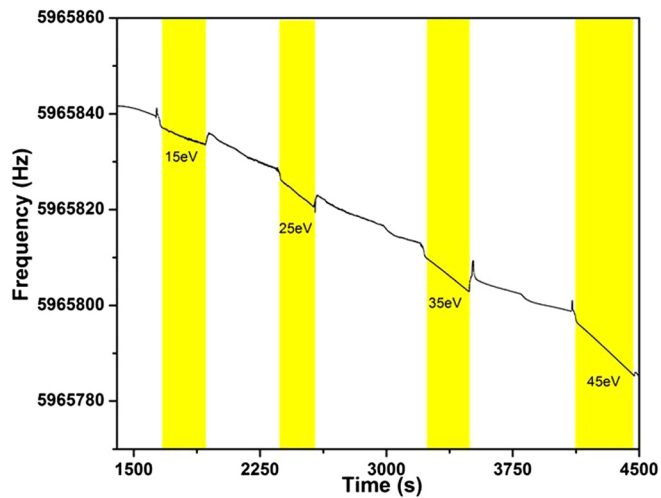


FIG. 5. QCM frequency change versus time during in-situ irradiation of GaSb samples at low energies (15, 25, 35, and 45 eV). Yellow regions show the change in the slope of the lines at each energy. The increase in the slope as the energy increases demonstrates an increase in the sputtering rate.

performed on a sample while being irradiated at 50 eV. The low energy used (50 eV) was chosen to monitor all growth stages of the structure. Figure 6 shows the real time GISAXS scans of the irradiated samples. In a GISAXS scan, the $q_{||} = 0$ peak is the specular beam.^{32,33} Peaks on each side of the specular region indicate correlated structure formation on the samples. The structures are separated by a real space distance of $\lambda = \frac{2\pi}{q_{||}}$. Four stages were observed during the structure growth. In the first stage, roughening of the sample occurred (Figure 6(a)) marked by the rise of the shoulder peak around the central peak^{34,35} and lasted up to 2750 s irradiation time (about $2.75 \times 10^{17} \text{ cm}^{-2}$). Since the sample had

a native oxide (was not oxygen free sample), roughening of the sample could be due to large Ga segregation of the surface during the early stage due to the native oxide layer. In the second stage (Figure 6(b)), the sample is smoothed again; and in the third stage (Figure 6(c)), correlation peaks began to grow demonstrating the formation of correlated nanostructures. The maximum intensity of the observed correlation peak was observed at 3300 s irradiation time or a fluence of $3.3 \times 10^{17} \text{ cm}^{-2}$. After that, the correlation peaks intensity dropped again (Figure 6(d)) suggesting a decrease in the nanostructures correlation (fourth stage). During the third stage (correlated structure formation), q values increased slightly (0.19 to 0.24) during the formation process. After that, the nanostructures showed little coarsening, and the $q_{||}$ value dropped to 0.22 which correspond to a real space distance of 28.5 nm. Figure 7(a) shows the SEM image of the sample after the irradiation. The distance between the nanostructures was about 25–30 nm in agreement with the GISAXS data. The intensity of the GISAXS patterns is proportional to the square of the Fourier transform (FFT) of the surface height.^{36–38} Figure 7(b) shows the FFT of the SEM image in Figure 7(e). The FFT image showed correlated peak of value of 0.2 in agreement with the GISAXS scans data. This demonstrates that the distance between nanostructures formed on GaSb during ion-beam irradiation varied during the growth with little coarsening. It should be noted, however, that the nanostructures observed in our work lacked the ordering observed by Facsko *et al.*⁷ Coarsening of the nanostructures was observed at high fluences and depended on energy (e.g., $2.5 \times 10^{17} \text{ cm}^{-2}$ at 500 eV) which also affects ordering. Such ordering could be possible through biasing the sample surfaces during ion beam bombardment. Investigation of the effect of biasing the sample

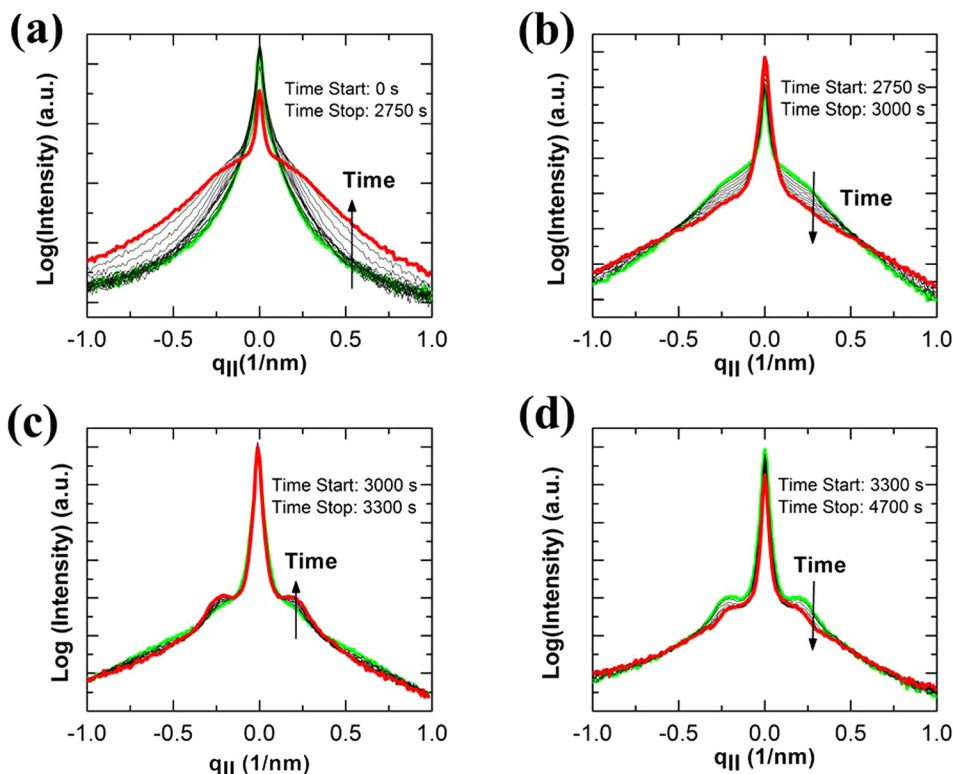


FIG. 6. Real time of GISAXS scans during nanostructures formation on GaSb substrates via 50 eV argon ion beam: (a) First stage: Roughing of the sample due to the sputtering of the native oxide and Ga segregation to the surface, (b) Second stage: Smoothing of the sample prior to structure formation (c) Third stage: Correlated structure formation (d) Fourth stage: Decrease in the correlation between the nanostructures.

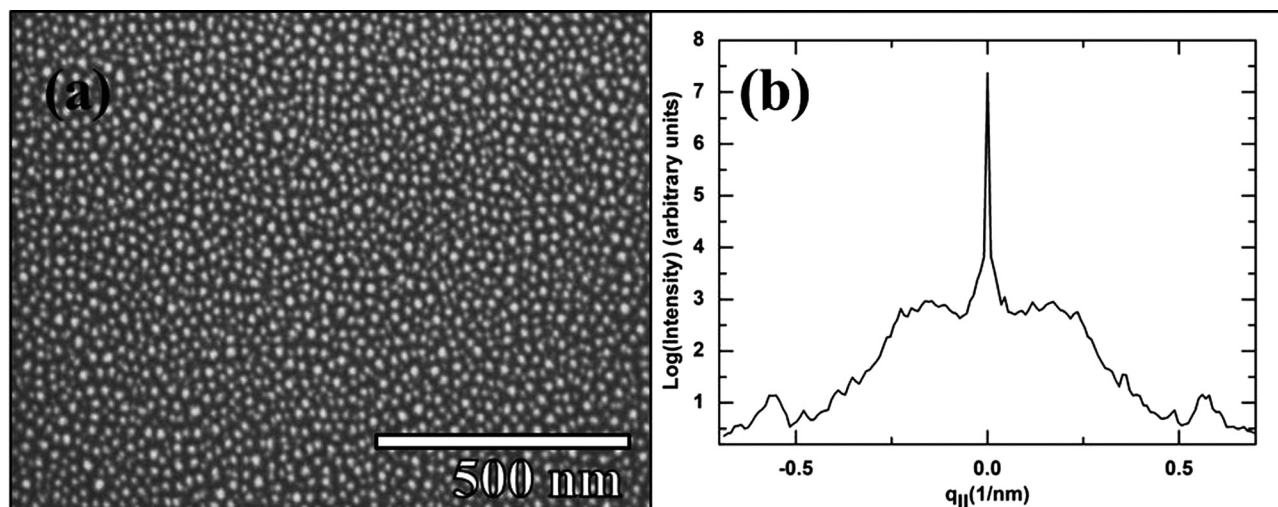


FIG. 7. (a) Scanning electron microscopy micrograph of the irradiated GaSb substrates by 50 eV argon ion beam during the real time GISAXS experiment. (b) FFT of (a) showing correlated structure formation in agreement with Figure 6(d).

surface is future work. However, our results indicate that at low energies (e.g., 25–45 eV) there is a wide range of fluences that produced well-structured dots and that their size can vary with irradiation fluence with no coarsening.

IV. CONCLUSIONS

In this work, several experiments were performed that enabled understanding of IBS nanopatterning at energies near threshold. The XPS and LEISS experiments demonstrated Ga enrichment on the surface prior to the nanostructure formation stage. The Ga enrichment was not due to Ga segregation or Ga₂O₃ formation since no oxygen was present on the samples at this stage. This result therefore is an indication that Sb is likely preferentially sputtered as corroborated by an *in-situ* collector experiment, and that the nanostructure formation mechanism is more likely to be driven by chemical instability and phase separation with Ga enrichment in the sub-surface in spite of Sb preferential sputtering. Moreover, the collector experiment also showed more Sb sputtering before and after nanostructure formation. Nanostructure formation at energies near sputtering (25 eV) threshold showed nanostructures formation with low-aspect ratio nanoscale dot morphology. Irradiations at 25 eV showed structures only on substrates that were oxygen-cleaned prior to irradiation. QCM measurements confirmed the occurrence of sputtering at these low energies. Irradiation of GaSb substrates at energies near sputtering threshold as well as high energies showed similar Ga relative composition behavior as a function of fluence demonstrating no sign of a mechanism difference if the nanopattern formation mechanism is mainly surface composition dependent. Real time GISAXS scans during ion beam irradiation of GaSb surfaces demonstrated that correlated nanostructure growth with little or no coarsening behavior at energies near sputtering threshold.

ACKNOWLEDGMENTS

This research was supported by US Army Medical Research Acquisition Activity (USAMRAA) under

W81XWH-11-2-0067 Grant, and the U.S. Department of Energy's 2010 Early Career Award DE-SC0004032. Use of the National Synchrotron Light Source, Brookhaven National Laboratory, was supported by the U.S. Department of Energy, Office of Science, Office of Basic Energy Sciences, under Contract No. DE-AC02-98CH10886. We would like to thank Professor Karl Ludwig and Dr. Alexander DeMasi for their assistance in performing and interpreting the GISAXS experiments, and Justin Fowler and Mohamad El Atwani for their efforts in the PRIHSM lab.

- ¹F. Frost, A. Schindler, and F. Bigl, *Phys. Rev. Lett.* **85**, 4116–4119 (2000).
- ²B. Ziberi, F. Frost, M. Tartz, H. Neumann, and B. Rauschenbach, *Appl. Phys. Lett.* **92**, 063102 (2008).
- ³A. Hanisch, A. Biermanns, J. Grenzer, S. Facsko, and U. Pietsch, *J. Phys. D: Appl. Phys.* **43**, 112001 (2010).
- ⁴C. Chappert, H. Bernas, J. Ferre, V. Kottler, J.-P. Jamet, Y. Chen, E. Cambril, T. Devolder, F. Rousseaux, V. Mathet, and H. Launois, *Science* **280**, 1919 (1998).
- ⁵R. Gago, L. Vázquez, R. Cuerno, M. Varela, C. Ballesteros, and J. M. Albella, *Appl. Phys. Lett.* **78**, 3316 (2001).
- ⁶O. El-Atwani, S. Ortoleva, A. Cimaroli, and J. P. Allain, *Nanoscale Res. Lett.* **6**, 403 (2011).
- ⁷S. Facsko, T. Dekorsy, C. Koerdts, C. Trappe, H. Kurz, A. Vogt, and H. L. Hartnagel, *Science* **285**, 1551 (1999).
- ⁸J. Muñoz-García *et al.*, "Self-organized surface nanopatterning by ion beam sputtering," in *Towards Functional Nanomaterials*, edited by Z. M. Wang (Springer, 2009).
- ⁹S. Facsko, H. Kurz, and T. Dekorsy, *Phys. Rev. B* **63**, 165329 (2001).
- ¹⁰R. Cuerno and A.-L. Barabási, *Phys. Rev. Lett.* **74**, 4746 (1995).
- ¹¹S. Facsko, T. Bobek, and H. Kurz, *Appl. Phys. Lett.* **80**(1), 130 (2002).
- ¹²J. F. Ziegler, SRIM-2008 software package, available online at www.srim.org.
- ¹³O. El-Atwani, J. P. Allain, A. Cimaroli, A. Suslova, and S. Ortoleva, *J. Appl. Phys.* **110**, 074301 (2011).
- ¹⁴S. Le Roy, E. Barthel, N. Brun, A. Lelarge, and E. Søndergård, *J. Appl. Phys.* **106**, 094308 (2009).
- ¹⁵S. Le Roy, E. Søndergård, I. S. Nerbø, M. Kildemo, and M. Plapp, *Phys. Rev. B* **81**, 161401(R) (2010).
- ¹⁶O. El-Atwani, J. P. Allain, and A. Suslova, *Appl. Phys. Lett.* **101**, 251606 (2012).
- ¹⁷P. D. Shipman and R. M. Bradley, *Phys. Rev. B* **84**, 085420 (2011).
- ¹⁸R. M. Bradley and P. D. Shipman, *Appl. Surf. Sci.* **258**, 4161–4170 (2012).
- ¹⁹S. Norris, e-print [arXiv:1205.6834v1 \[cond-mat.mtrl-sci\]](https://arxiv.org/abs/1205.6834v1) (2012).

- ²⁰E. Papis, A. Kudla, T. T. Piotrowski, K. Golaszewska, E. Kaminska, and A. Piotrowska, *Mater. Sci. Semicond. Process.* **4**, 293 (2001).
- ²¹C. Palacio, J. Olvera, J. L. Plaza, and E. Dieguez, *Surf. Coat. Technol.* **206**, 3146 (2012).
- ²²W. Yu, J. L. Sullivan, and S. O. Saied, *Surf. Sci.* **352–354**, 781–787 (1996).
- ²³G. P. Schwartz, G. J. Gualtieri, G. W. Kammlott, and B. Schwartz, *J. Electrochem. Soc.* **126**, 1737 (1979).
- ²⁴O. El-Atwani, J. P. Allain, and S. Ortoleva, *Nucl. Instrum. Methods Phys. Res. B* **272**, 210–213 (2012).
- ²⁵R. H. H. Smits, K. Seshan, J. R. H. Ross, L. C. A. van den Oetelaar, J. H. J. M. Helwegen, M. R. Anantharaman, and H. H. Brongersma, *J. Catal.* **157**, 584–591 (1995).
- ²⁶C. J. Jenks, A. R. Ross, T. A. Lograsso, J. A. Whaley, and R. Bastasz, *Surf. Sci.* **521**, 34–42 (2002).
- ²⁷O. El-Atwani, S. Gonderman, A. DeMasi, F. Bedoya, K. Ludwig, and J. P. Allain, “The effect of incident ion mass on GaSb nanopatterning studied by *in-situ* X-ray studies” (unpublished).
- ²⁸R. M. Bradley and J. M. E. Harper, *J. Vac. Sci. Technol. A* **6**, 2390 (1988).
- ²⁹R. Kelly, *Surf. Interface Anal.* **7**, 1 (1985).
- ³⁰A. Galdikas and L. Praniavichius, *Interaction of Ions with a Condensed Matter* (Nova Science Pub. Inc., 2000), Vol. 229.
- ³¹I. S. Nerbo, S. Le Roy, M. Foldyna, E. Sondergard, and M. Kildemo, *Opt. Express* **19**(13), 12551 (2011).
- ³²G. Renaud, R. Lazzari, and F. Leroy, *Surf. Sci. Rep.* **64**, 255–380 (2009).
- ³³S. K. Sinha, E. B. Sirota, S. Garoff, and H. B. Stanley, *Phys. Rev. B* **38**, 2297 (1988).
- ³⁴G. Ozaydin, K. F. Ludwig, H. Zhou, L. Zhou, and R. L. Headrick, *J. Appl. Phys.* **103**, 033512 (2008).
- ³⁵G. Ozaydin, K. F. Ludwig, H. Zhou, and R. L. Headrick, *J. Vac. Sci. Technol. B* **26**, 551 (2008).
- ³⁶A. Guenterschulze and W. V. Tollmien, *Z. Phys.* **119**, 685 (1942).
- ³⁷G. Ozaydin, A. Ozcan, Y. Wang, K. F. Ludwig, Jr., H. Zhou, and R. Headrick, *Nucl. Instrum. Methods Phys. Res. B* **264**, 47 (2007).
- ³⁸G. Ozaydin, A. Ozcan, Y. Wang, K. F. Ludwig, Jr., H. Zhou, R. Headrick, and P. Siddons, *Appl. Phys. Lett.* **87**, 163104 (2005).